J Mater Sci (2018) 53:6980–6990

Metals

Shear localization and size-dependent strength of YCd_6 quasicrystal approximant at the micrometer length scale

Gyuho Song[1,*], Tai Kong[2], Keith J. Dusoe[1], Paul C. Canfield[2], and Seok-Woo Lee[1]

[1] Department of Materials Science and Engineering and Institute of Materials Science, University of Connecticut, 97 North Eagleville Road, Unit 3136, Storrs, CT 06269-3136, USA

[2] Ames Laboratory, U.S. DOE and Department of Physics and Astronomy, Iowa State University, Ames, IA 50011, USA

Received: 9 November 2017
Accepted: 15 January 2018
Published online: 24 January 2018

ABSTRACT

Mechanical properties of materials are strongly dependent of their atomic arrangement as well as the sample dimension, particularly at the micrometer length scale. In this study, we investigated the small-scale mechanical properties of single-crystalline YCd_6, which is a rational approximant of the icosahedral Y-Cd quasicrystal. In situ microcompression tests revealed that shear localization always occurs on {101} planes, but the shear direction is not constrained to any particular crystallographic directions. Furthermore, the yield strengths show the size dependence with a power law exponent of 0.4. Shear localization on {101} planes and size-dependent yield strength are explained in terms of a large interplanar spacing between {101} planes and the energetics of shear localization process, respectively. The mechanical behavior of the icosahedral Y-Cd quasicrystal is also compared to understand the influence of translational symmetry on the shear localization process in both YCd_6 and Y-Cd quasicrystal micropillars. The results of this study will provide an important insight in a fundamental understanding of shear localization process in novel complex intermetallic compounds.

Introduction

Novel complex intermetallic compounds often possess superior chemical, physical, electronic, and magnetic properties due to their unique atomic arrangements and have been regarded as an excellent candidate material for future devices [1–7]. However, their extreme brittleness at room temperature significantly limits their practical applications. Therefore, it is important to enhance their ductility as well as to understand a potential plasticity mechanism if available. In general, fracture of brittle materials is greatly sensitive to the geometry and distribution of defects, for instance, surface flaws or microcracks [8]. Plastic deformation in these materials is often obscured by stress concentration followed

Address correspondence to E-mail: gyuho.song@uconn.edu

https://doi.org/10.1007/s10853-018-2043-8

by brittle fracture at a stress level lower than yield strength. If the defects can be effectively removed, however, it would be possible to observe the ductility of these otherwise brittle materials. Recent studies on small-scale mechanics revealed that size reduction is a great way to enhance the ductility because the probability to contain a defect in a smaller volume is statistically lower. If the dimension of materials becomes close, especially, to the micro-/nano-meter length scale, they would possess nearly no significant defects, and it would be possible to avoid stress concentration as well as catastrophic failure. Then, it is possible to study the intrinsic plastic deformation process in novel intermetallic compounds even at room temperature.

For the last decade, micropillar compression and tension tests have been extensively used to investigate the size effects on the mechanical properties of materials [9–17]. Recent studies successfully demonstrated that a brittle material could become more ductile when its dimension is reduced down to the micro-/nano-meter length scale. Gallium arsenide (GaAs) micropillars with 1 μm in diameter display significant dislocation-based plasticity, which was confirmed by post-deformation transmission electron microscope (TEM) analysis [18]. Silicon nanopillars with diameters less than 300 nm exhibit extensive plastic slip events instead of brittle fracture under uniaxial compression [19]. This work showed that size reduction to a certain critical diameter induces the brittle-to-ductile transition. More notably, icosahedral Al-Pd-Mn quasicrystal (QC) nanopillars also exhibit the brittle-to-ductile transition at the diameter between 350 and 510 nm despite the absence of translational symmetry in its quasicrystalline structure [20]. Their in situ TEM deformation suggested that icosahedral Al-Pd-Mn QC nanopillars might exhibit dislocation climb and glide even at room temperature, which contribute to room temperature ductility at small length scales. As another special case, Zr-based bulk metallic glass (BMG) nanopillars of 100 nm in diameter, which has an amorphous atomic arrangement, exhibit even tensile ductility at room temperature [21]. All these results confirm that size reduction is indeed able to prevent catastrophic failure and can promote plastic deformation, enabling the study of intrinsic plastic deformation behavior of materials, which are usually brittle at bulk scale.

Among all of the studies listed above, the deformation behaviors of QCs and BMGs seem to be unique, compared to those of crystalline materials since they exhibit small-scale plasticity even without the aid of translational symmetry. Translational symmetry is usually required for a material to exhibit conventional dislocation glide process, which would be the most effective plasticity mechanism in crystalline materials. The absence of translational symmetry operates alternative plasticity mechanism, for instance, dislocation climb in QCs or shear banding in BMGs. The translational symmetry would be an important factor to control the deformation process in brittle materials at small length scales. Thus, it would be worthwhile to investigate how the translational symmetry plays a role in the deformation process in novel intermetallic compounds to gain a deeper understanding of their plasticity mechanisms.

In order to examine the role of translational symmetry in mechanical properties of intermetallic compounds, QC would be an excellent system to study because some QCs have a quasicrystal approximant (QCA), a chemical counterpart that possesses not only the same repeating unit cluster, but also translational symmetry [22]. Both QC and QCA are usually extremely brittle intermetallic compounds due to the directionality of their atomic bonds and complex atomic configurations. If they can exhibit some amount of plasticity by reducing the sample dimension, however, it would be possible to study how both translational symmetry and sample dimension influences their mechanical behaviors.

Recently, we successfully grew both QC (i-YCd or $YCd_{7.48}$) and QCA (YCd_6) through solution growth of Y-Cd binary system. YCd_6 QCA has the same Tsai-type icosahedral cluster with i-YCd QC but has the body-centered-cubic array of these clusters, which produces translational symmetry [22, 23]. In this study, we fabricated micropillars with various diameters and investigated the effects of translational symmetry and sample dimension on the mechanical properties, primarily, of YCd_6 QCA by using in situ microcompression. We found that all YCd_6 QCA micropillars with diameters ranging from 0.3 to 10 μm exhibit shear localization on {101} planes, and shear displacement always occurs along the maximum shear stress direction. The i-YCd QC micropillars also exhibit shear localization but only at the submicrometer scale. The i-YCd QC micropillars with a few μm in diameter display catastrophic failure. We

also observed size-dependent yield strength of YCd_6 QCA micropillars with the power law exponent of 0.4. We discuss shear localization on {101} planes and size-dependent yield strength of YCd_6 QCA micropillars in terms of a large interplanar spacing between {101} planes and the energetics of shear localization process, respectively. We believe that the results of our study will provide an important insight in a fundamental understanding of deformation processes in novel complex intermetallic compounds.

Materials and methods

Solution growth of the YCd_6 quasicrystal approximant and i-YCd quasicrystal

Single-crystalline YCd_6 QCA and grains of i-YCd QC crystals were grown from a Cd-rich melt using a high-temperature solution growth method [23]. Starting bulk elements, with molar ratios of Y/Cd = 0.8:99.2 (for i-YCd) and 7:93 (for YCd_6), were packed in a frit-disk alumina crucible set [24] and sealed in a silica ampoule under a partial argon atmosphere. The ampoule was then heated up to 700 °C, dwelt there for 10 h, and slowly cooled to 500 °C for the QCA and 335 °C for QC, at which temperature the remaining liquid was quickly decanted in a centrifuge. The single crystal specimen of YCd_6 exhibits clear {001} rectangular facets and {101} hexagonal facets, which enable us to identify the crystallographic directions of the sample relatively easily (Fig. 1a). In the case of the i-YCd QC, we obtained an agglomerate of several grains, and each grain was large enough to make multiple micropillars (Fig. 1b). We fabricated micropillars along a [211111] direction on the pentagon-shaped plane, which has fivefold rotational symmetry (the inset of Fig. 1b).

Micropillar fabrication and in situ micropillar compression of YCd_6

Micropillars were fabricated by using a Ga^+ focused ion beam (FIB) technique (Helios Nanolab 460F1, FEI, USA). Initially, currents of ~ 21 nA were used to mill craters large enough to view the pillars during the compression. Next, the target-sized micropillars were obtained by milling with lower currents ranging from 80 to 7.7 pA in order to minimize ion beam damage (Fig. 1c). The ratio of height to diameter of micropillars usually remained below 5. The taper angle was always less than 2°, which is small enough to assume that the taper effect on the stress distribution is not significant. In fact, we found that during compression, a shear localization trace is formed at random places in YCd_6 QCA micropillar, implying that the taper effect is indeed negligible in our study. We made [001]-oriented YCd_6 QCA micropillars with various diameters (0.2–10 μm) to investigate the deformation behavior and the size dependence of yield strength. We also created [115]-oriented YCd_6 QCA micropillars to check if shear direction is constrained to any particular crystallographic directions. [211111]-oriented i-YCd QC nanopillars were also fabricated to examine how translational symmetry influences the plasticity or fracture behavior of YCd_6 QCA. All the micropillars in this study were tested under in situ uniaxial compression (NanoFlip,

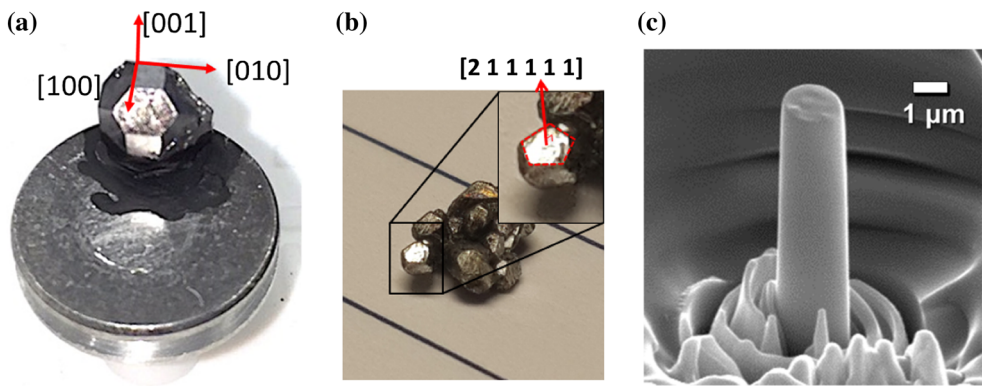

Figure 1 **a** Optical photograph of YCd_6 QCA single crystal. The crystallographic direction can be easily derived from the shape of single crystal; **b** optical photograph of single grained i-YCd QC agglomerates. Micropillars were fabricated along a [211111] direction, about which there is the fivefold rotation symmetry (See the pentagon-shaped flat surface in the inset); **c** [001]-oriented YCd_6 QCA micropillar with the top diameter of 1.7 μm.

Nanomechanics, Inc, USA) at room temperature in a scanning electron microscope (JEOL 6330F FEG SEM, JEOL, Japan). The nominal strain rate was $\sim 10^{-3}$ s^{-1} using a load control feedback system. We carefully examined in situ videos, which are recorded during a mechanical test, to determine whether a strain burst results from shear localization or catastrophic brittle failure. Pre-/post-deformation observations were also done using a scanning electron microscope (SEM) (Helios Nanolab 460F1 and Teneo LVSEM, FEI, USA).

Results and discussion

Confined shear localization process in YCd_6 QCA micropillars

Representative stress–strain curves (among the total 20 samples) of YCd_6 micropillars with different diameters are shown in Fig. 2a. Most samples show large strain bursts right after yielding. We confirmed from in situ movies and post-deformation images that these strain bursts do not result from brittle fracture but shear displacement (Fig. 2b). All twenty [001]-oriented YCd_6 micropillars in this study exhibit shear displacement traces on specific crystallographic planes without catastrophic failure. According to the reference crystallographic coordinate system (Figs. 1a, 2c), we can find four {101} planes (A, B, C and D) around a (001) plane, and we confirmed that the observed shear displacement traces in YCd_6 QCA micropillars correspond exactly to these four {101} planes (Fig. 3). Furthermore, all shear deformation

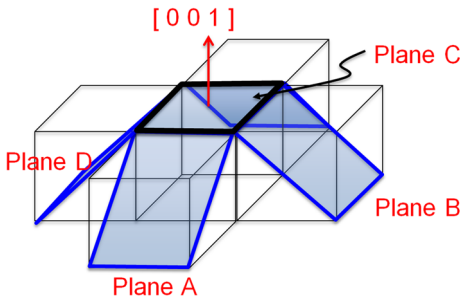

Figure 3 Schematic diagram of {101} planes of YCd_6 QCA. Plane A, B, C and D correspond to those in Fig. 2c.

events occur along <10$\bar{1}$> directions, which correspond to the maximum shear stress direction under the [001] loading.

The YCd_6 QCA has 168 atoms in a single unit cell, which is the consequence of body-centered-cubic array of Tsai-type icosahedral clusters (Fig. 4a) [25]. This atomic arrangement appears to be much more complicated than any monatomic metallic systems. Thus, it would be challenging to perform computer simulations to understand the shear displacement process in YCd_6 QCA. For instance, density functional theory calculations of general stacking fault energies would be computationally expensive due to the large number of atoms in a single unit cell. Furthermore, up to our knowledge, there is no reliable pair potential to reproduce the crystal structure of YCd_6 QCA. Thus, it is difficult to perform molecular dynamic simulation, too. Although advanced computer simulations cannot be done easily, however, the careful examination of the YCd_6 QCA crystal structure can still provide an important insight to understand how YCd_6 QCA can have preferred

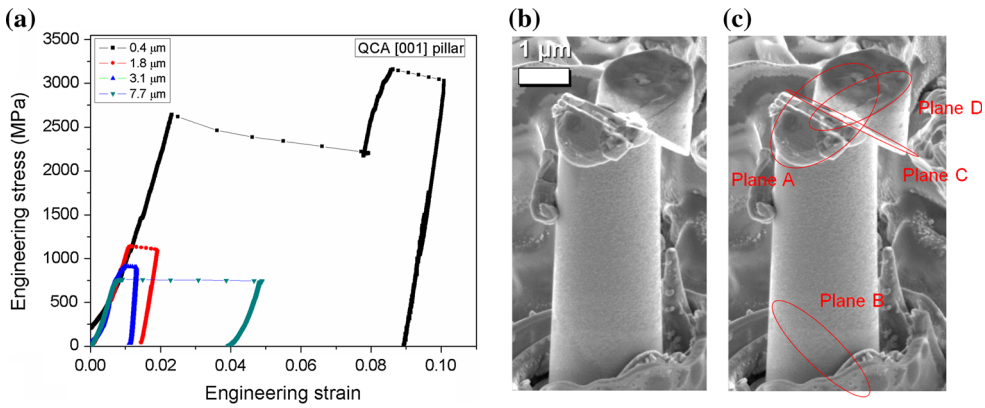

Figure 2 **a** Representative engineering stress–strain data of YCd_6 QCA micropillars with four different diameters. We tested the total 20 micropillars (See Fig. 7); **b** post-deformation SEM image of YCd_6 QCA micropillar after uniaxial compression; **c** shear localization traces of YCd_6 QCA micropillar. Note that shear localization occurs on four different {101} planes (A, B, C and D).

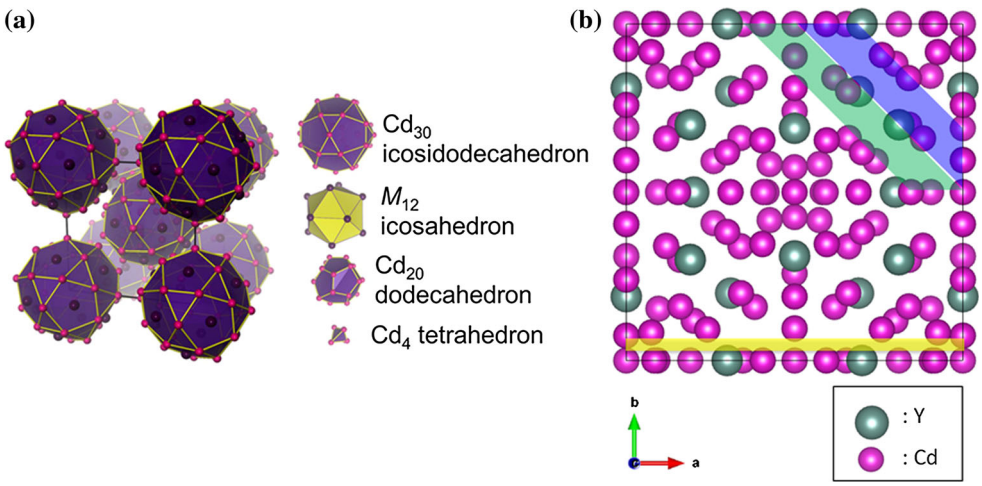

Figure 4 **a** Body-centered-cubic array of icosahedra clusters in YCd_6 unit cell (Reprinted with the permission of Nishimoto et al. [25], copyright 2013, Journal of Physics: Condensed Matter) **b** [100] view of YCd_6 unit cell. Note that {101} planes have two sets of large interplanar spacings (blue and green section). Yellow section shows the large interplanar spacing between {001} planes.

crystallographic planes, where shear displacement occurs. Figure 4a shows the complexity of atomic configuration of YCd_6 QCA. In a [100] view of unit cell, however, one can clearly see a large interplanar spacing of {101} and {001} planes (Fig. 4b). It is not easy to mathematically define their interplanar spacing due to the rough and complex atomic distributions on each crystallographic plane, but there are certainly large empty spaces which are parallel to {101} and {001} planes (blue and green sections for $\{10\bar{1}\}$ and yellow section for {001} in Fig. 4b. Particularly, for {101} planes, there are two sets of large interplanar spacings. Typically, plastic slip in a crystalline material occurs more preferentially on a crystallographic plane with the largest interplanar spacing because these planes are usually the most weakly bonded to each other. Under uniaxial deformation along the [001] direction, the shear stress on a {001} plane is zero. Therefore, {101} planes would be crystallographically preferable for shear deformation process in our study. However, it is uncertain which set of planes (blue and green in Fig. 4b) produces the shear deformation traces observed in this study.

Furthermore, we found that the shear displacement always occurs along a $<10\bar{1}>$ direction, which corresponds to the maximum shear stress direction on {101} planes under the current [001] loading condition. Note that the shear displacement direction does not always follow the direction of the maximum shear stress on a given plane. For instance, a dislocation slip usually occurs in a slip system that has the maximum Schmid factor, which does not necessarily correspond to the maximum shear stress direction on a given slip plane. Therefore, our observation of the shear displacement direction, $<10\bar{1}>$, in YCd_6 QCA micropillars is not sufficient enough to determine whether a shear deformation in our study occurs according to the maximum Schmid factor (dislocation plasticity) or not. Due to the large size of the unit cell and its complex atomic arrangement, the magnitude of the Burgers vector along a $<10\bar{1}>$ direction is $\sim$ 13 angstroms, which is unusually large. Thus, dislocation slip is unlikely to occur.

In order to confirm if a dislocation process controls the observed deformation process or just the maximum shear stress does, we also created a [115] micropillar, an orientation, which is slightly deviated (15.8°) from a [001] direction, and performed uniaxial compression tests (Fig. 5a). In the case of [115] micropillar compression, a shear deformation on a {101} plane was observed again, but occurred along the $[2\bar{1}\bar{2}]$ direction, which is still the maximum shear direction on a {101} plane under [115] loading (Fig. 5a, c). Therefore, a shear deformation plane is always constrained to {101} planes, but a shear direction seems to follow the maximum shear direction only. It is worth noting that the shortest translational vector on {101} plane is $<1\bar{1}\bar{1}>$, which has the Schmid factor of 0.45 for a {101} plane and [115] loading. Under the same loading condition, the Schmid factor of $<2\bar{1}\bar{2}>$ {101} system is 0.47. Considering the small difference in Schmid factor and the huge difference in magnitude of the translational vector (Fig. 5b), a slip would occur in $<1\bar{1}\bar{1}>$ {101} if a dislocation slip is a dominant process. However, our observation of $<2\bar{1}\bar{2}>$ {101} implies that shear deformation always prefers the maximum shear stress direction.

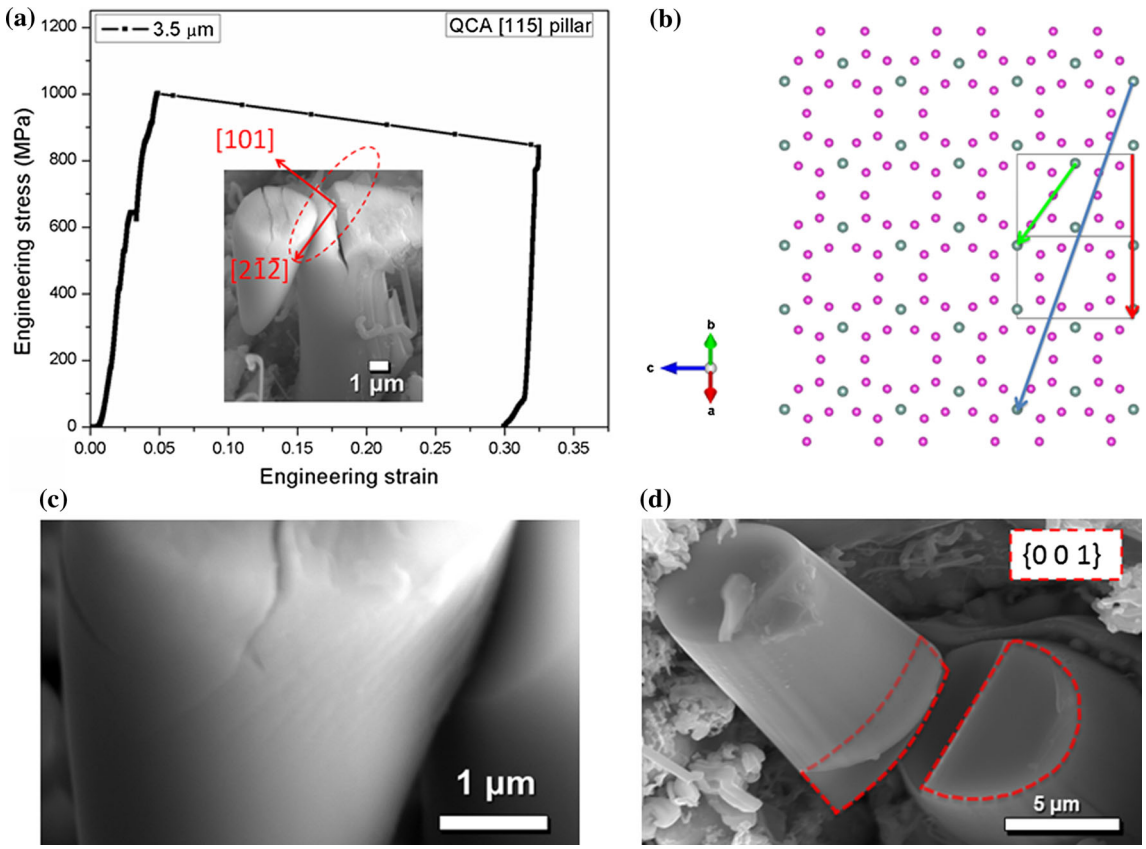

Figure 5 **a** Engineering stress–strain data of [115]-oriented YCd_6 micropillar. The inset shows the postmortem SEM image. The deformation direction shows that shear localization occurs along the maximum shear stress direction, which is different from the shear localization direction of [001]-oriented micropillar; **b** [2$\bar{1}\bar{2}$] slip vector on a {101} plane; **c** the shear localization traces on {101} plane; **d** the cleavage on a (001) plane due to the bending moment at the pillar bottom.

Although YCd_6 micropillar is crystalline, the complexity of its atomic configuration would make it nearly behave like BMGs. Its large unit cell size and complex atomic configurations would prefer shear localization to conventional dislocation plasticity. Thus, shear deformation in YCd_6 micropillars would be similar with shear banding in BMGs [26, 27], but an unusually wide interplanar spacing of {101} planes would provide a geometrical constraint of this shear deformation. In sum, it would be more appropriate to describe the deformation behavior in YCd_6 as 'shear localization,' which is confined to {101} planes.

Note that the observed deformation mode does not lead to complete fracture but finite plastic strain. This observation is also similar with a stopped shear bands in ductile BMGs under compression. These stopping behaviors of shear localization in our materials or shear bands in BMGs are related to the amount of elastic strain energy, machine stiffness, and the internal friction [28]. In the current study, it would be difficult to identify the major reasons for stopping shear localization process, and a further analysis is required.

We sometimes found that clean cleavage occurs on a (001) plane (Fig. 5d). This cleavage occurs due to the bending moment near the pillar bottom, which is caused by off-axis compression right after significant shear displacement occurs. This would also be related to a large interplanar spacing between {001} planes, which would be weakly bonded. Note that the axial splitting cracks, which are parallel to the loading direction, are also formed (Fig. 5a). Once shear displacement occurs, the top part slides down. Then, the bottom part of micropillar has the tilted surface. Further loading pushes the top part and the bottom part along the laterally opposite directions and develops the tensile stress component, which is perpendicular to the loading direction. Then, axial splitting cracks can be formed. The formation of axial

splitting cracks has been commonly observed in micropillar compression of brittle materials [29].

Comparison of small-scale mechanical behavior between YCd_6 QCA and i-YCd QC

The benefit of translational symmetry in shear localization process of YCd_6 QCA was investigated by comparing with the mechanical behavior of i-YCd QC, which has the same icosahedral clusters but no translational symmetry. We performed micropillar compression test on two different sized i-YCd QC micropillars (0.4 and 4.4 μm in diameter). Similar to Al-Pd-Mn QC, we found that i-YCd QC micropillars show the transition from brittle-to-ductile deformation by size reduction (Fig. 6). Fracture right after yielding for i-YCd QC micropillars with 4.4 μm in diameter (Fig. 6b), but sub-micrometer size pillar with 0.4 μm in diameter exhibit shear deformation behavior with finite plastic strain (Fig. 6c). Al-Pd-Mn QC nanopillar works postulated that dislocation climb and glide would control its plasticity at the sub-micrometer length scale [20]. As seen in our comparative study between [001] and [115] loading on YCd_6 QCA micropillars, a complex atomic arrangement in YCd_6 QCA prefers shear localization process in spite of its translational symmetry. So, we conclude that our i-YCd QC, which even lacks translational symmetry, is unlikely to exhibit the dislocation-mediated process, and its plasticity would be controlled by shear localization process, too.

Both YCd_6 QCA and i-YCd QC micropillars seem to exhibit similar shear localization behavior, but the critical diameter of brittle-to-ductile transition is different. Note that YCd_6 QCA micropillars exhibit shear localization process up to 10 μm. We were not able to study an YCd_6 QCA micropillar with diameter larger than 10 μm due to the maximum force limit of our equipment. However, i-YCd QC micropillar with 4.4 μm in diameter exhibits brittle fracture, so the critical diameter of brittle-to-ductile transition of i-YCd QC must be less than 4.4 μm. Thus, the critical diameter of brittle-to-ductile transition of YCd_6 QCA is much larger than that of i-YCd QC.

YCd_6 QCA and i-YCd QC have the same Tsai-type unit cluster, so the short-range atomic arrangement would be similar. However, the long-range atomic

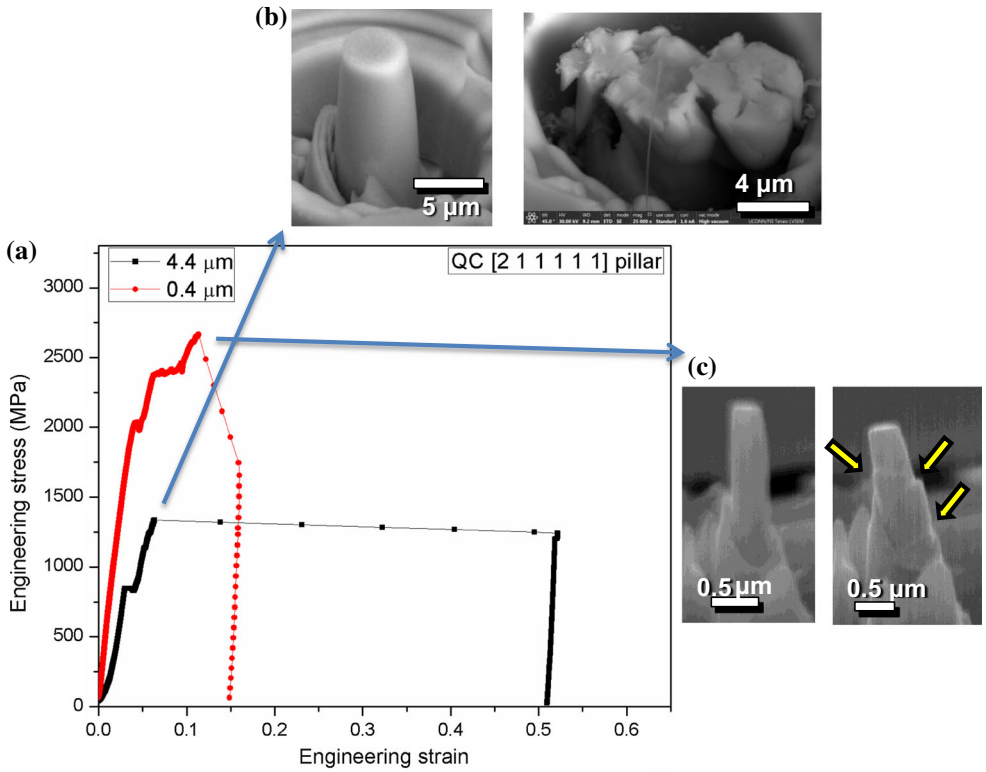

Figure 6 **a** Representative engineering stress–strain data of i-YCd QC micropillars; **b** SEM images of a 4.4 μm diameter pillar before and after compression test; **c** SEM images of 0.4 μm diameter pillar before and after compression test.

arrangements are different because body-centered-cubic array of unit clusters in QCA is completely different from icosahedral array in QC. This large difference should affect the critical diameter of brittle-to-ductile transition. Due to the large interplanar spacing of {101} planes, YCd_6 QCA is able to show the easier and more stable shear localization even in a larger micropillar. However, i-YCd QC requires the more significant size reduction because there is no easy path of shear localization. In this case, collective atomic rearrangement under the maximum shear stress would create the shear displacement traces. This deformation mode would be similar with BMGs, which has no defined crystallographic plane, too, and becomes more ductile as the diameter decreases.

Size effects on yield strength of YCd_6

Strength of materials at small length scales is often size-dependent [30–34], and it is important to understand how strength changes with sample dimension, especially at the micrometer length scale. In this study, we investigated the yield strength of [001] YCd_6 QCA micropillars as a function of diameter, and it is apparent that the yield strength increases as the micropillar diameter decreases (Fig. 7). Thus, YCd_6 micropillars exhibits '*Smaller is Stronger*' behavior. The power law exponent is close to 0.4 when a size-dependent yield strength (σ) is described by $\sigma = C \cdot D^{-n}$, when C is the prefactor, D is the diameter, and n is the exponent. Single-crystalline metallic micropillars usually exhibit a size-dependent strength due to dislocation source-controlled plasticity. As the sample dimension becomes smaller, the higher stress is required to operate a preexisting dislocation source, for instance, either a single-arm dislocation source or surface dislocation source [35, 36]. As discussed in Sect. 3.1, however, our YCd_6 QCA micropillars do not seem to exhibit dislocation plasticity, and shear localization would be a dominant deformation process. The shear localization mechanism is analogous to shear band mechanism in BMGs since shear bands are formed along the maximum shear stress direction. The only difference is that, in our case, shear localization is constrained to {101} planes while BMGs have no defined crystallographic plane where shear band is formed. However, the similar model can be applied to both YCd_6 QCA and BMG systems because the energetics of shear localization in YCd_6 would be similar to that of shear banding.

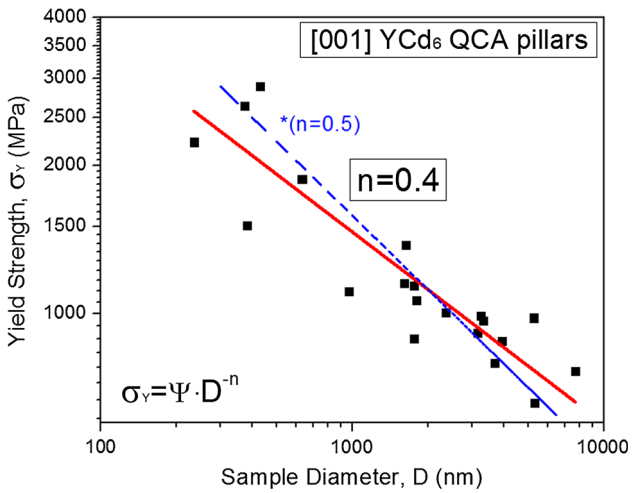

Figure 7 A plot of yield strength of [001] YCd_6 QCA micropillars as a function of sample diameter. Blue broken line shows the theoretically estimated exponent of 0.5.

The shear band model has been widely used to understand the size effect in BMGs. Volkert, et al. derived a power law relation in BMGs by applying the Griffith's crack equation to the shear band model [37], and Wang, et al. predicted the theoretical power law exponent of BMGs to be 0.5 [38]. Jang et al. also used the shear crack model to determine the critical diameter for brittle-to-ductile transition of Zr-based BMGs [21]. In the shear band model, Volkert et al. and Wang et al. replaced 'the energy increase by creating the exposed surfaces (surface energy)' in the Griffith's theory with 'the energy increased by the formation of shear band (shear band energy).' Reconfiguration of random atomic configuration and the increase in free volume in shear band contributes to the increase in total free energy of system. In the case of YCd_6 micropillars, shear localization on {101} planes would create the significant atomic misfit, which also results in the increase in total free energy. This analogy allows us to adapt the shear band model suggested by Volkert et al. and Wang et al. as discussed in our manuscript.

For our materials, with conservation of energy assumed [37–39], at the moment of shear localization, the stored elastic energy up to yielding is transferred to the atomic misfit energy on a {101} plane where the preferential shear localization occurs. This situation is similar with shear band process in BMGs, which creates the shear band energy due to atomic reconfigurations and free volume creation in a thin shear

band region. Based on this analogy, therefore, it is expected therefore, it is expected that the scaling exponent of YCd_6 would be close to 0.5 of BMGs. Note that our observation (0.4) is relatively close to this theoretical estimation, implying indirectly that the shear band model works for our case. The small deviation from 0.5 may be attributed to other losses (i.e., heat dissipation and elastic recovery) because the exponent of 0.5 is derived based on the assumption of complete energy transfer from elastic strain energy to atomic misfit energy.

Concluding remarks

In this study, we investigated shear localization behavior and size-dependent yield strength of YCd_6 QCA micropillars. The YCd_6 QCA forms shear localization traces under [001] uniaxial compression in the entire range of the pillar size from 0.2 to 9 μm. The shear localization traces always corresponds to {101} planes, but a shear localization direction does not seem to be constrained to any particular crystallographic direction. We confirmed that shear localization always occurs along the direction of the maximum shear stress on {101} planes and does not follow the Schmid law of dislocation plasticity. Crystal structure analysis shows that YCd_6 QCA possesses large interplanar spacing between {101} planes that would provide the geometrical confinement of shear localization. Also, we also found that i-YCd QC micropillars show the transition from brittle-to-ductile deformation by size reduction, but the critical diameter of brittle-to-ductile transition in YCd_6 QCA should be larger than i-YCd QC. These results imply that a translational symmetry is important to show a ductile-like shear localization process in Y-Cd system. We also observed size-dependent yield strength with the power law exponent of 0.4. According to the energetics of shear localization, the scaling exponent is expected to be 0.5, which is close to our experimental observation (0.4). The slight deviation from 0.5 would result from inevitable energy losses such as elastic recovery and heat dissipation. We believe that our results will provide an insight in understanding the effects of translational symmetry and sample dimension on deformation process in novel complex intermetallic compounds.

Acknowledgements

The authors gratefully acknowledge the financial support of UConn Start-Up Grant. FIB works were performed using the facilities in the UConn/FEI Center for Advanced Microscopy and Materials Analysis (CAMMA). Work by P.C. Canfield and T. Kong was supported by the U.S. Department of Energy, Office of Basic Energy Science, Division of Materials Sciences and Engineering. Their research was performed at the Ames Laboratory. Ames Laboratory is operated for the U.S. Department of Energy by Iowa State University under Contract No. DE-AC02-07CH11358.

References

[1] Gschneidner K, Russell A, Pecharsky A, Morris J, Zhang Z, Lograsso T, Hsu D, Lo CC, Ye Y, Slager A (2003) A family of ductile intermetallic compounds. Nat Mater 2(9):587–591

[2] Russell AM (2003) Ductility in intermetallic compounds. Adv Eng Mater 5(9):629–639

[3] Inoue A, Kimura H, Masumoto T (1987) Formation of Al-Cr-Si quasicrystal with high silicon concentration by rapid quenching and its thermal and electrical properties. J Mater Sci 22(5):1864–1868. https://doi.org/10.1007/BF01132418

[4] Bolmaro R, Povolo F (1989) Elastic and anelastic behaviour of icosahedral quasicrystals. J Mater Sci 24(8):2975–2980. https://doi.org/10.1007/BF02385656

[5] Wolf B, Swain M, Kempf M, Paufler P (2000) A comparison of indentations of different size and geometry in single-quasicrystalline AlPdMn. J Mater Sci 35(3):723–734. https://doi.org/10.1023/A:1004713502703

[6] Bandyopadhyay P, Kern P, Siegmann S (2004) Corrosion behavior of vacuum plasma sprayed Ti-Zr-Ni quasicrystal coatings. J Mater Sci 39(19):6101–6104. https://doi.org/10.1023/B:JMSC.0000041711.82764.68

[7] Tanabe T, Kameoka S, Tsai AP (2011) Evolution of microstructure induced by calcination in leached Al–Cu–Fe quasicrystal and its effects on catalytic activity. J Mater Sci 46(7):2242–2250. https://doi.org/10.1007/s10853-010-5063-6

[8] Meyers MA, Chawla KK (2009) Mechanical behavior of materials, vol 2. Cambridge University Press, Cambridge

[9] Nix WD, Greer JR, Feng G, Lilleodden ET (2007) Deformation at the nanometer and micrometer length scales: effects of strain gradients and dislocation starvation. Thin Solid Films 515(6):3152–3157

[10] Budiman A, Han S, Greer J, Tamura N, Patel J, Nix W (2008) A search for evidence of strain gradient hardening in

Au submicron pillars under uniaxial compression using synchrotron X-ray microdiffraction. Acta Mater 56(3):602–608

[11] Lee S-W, Han SM, Nix WD (2009) Uniaxial compression of fcc Au nanopillars on an MgO substrate: the effects of pre-straining and annealing. Acta Mater 57(15):4404–4415

[12] Cui Y, Po G, Ghoniem N (2016) Temperature insensitivity of the flow stress in body-centered cubic micropillar crystals. Acta Mater 108:128–137

[13] Kiener D, Minor A (2011) Source truncation and exhaustion: insights from quantitative in situ TEM tensile testing. Nano Lett 11(9):3816–3820

[14] Wang S, Yang Y, Zhou L, Mai Y-W (2012) Size effect in microcompression of epoxy micropillars. J Mater Sci 47(16):6047–6055. https://doi.org/10.1007/s10853-012-6513-0

[15] Yang Y, Liu CT (2012) Size effect on stability of shear-band propagation in bulk metallic glasses: an overview. J Mater Sci 47(1):55–67. https://doi.org/10.1007/s10853-011-5915-8

[16] Yu J, Wu J, Yu L, Yang H, Kao C (2017) Micromechanical behavior of single-crystalline Cu6Sn5 by picoindentation. J Mater Sci 52(12):7166–7174. https://doi.org/10.1007/s10853-017-0952-6

[17] Huskins EL, Cordero ZC, Schuh CA, Schuster BE (2015) Micropillar compression testing of powders. J Mater Sci 50(21):7058–7063. https://doi.org/10.1007/s10853-015-9260-1

[18] Michler J, Wasmer K, Meier S, Östlund F, Leifer K (2007) Plastic deformation of gallium arsenide micropillars under uniaxial compression at room temperature. Appl Phys Lett 90(4):3123

[19] Östlund F, Rzepiejewska-Malyska K, Leifer K, Hale LM, Tang Y, Ballarini R, Gerberich WW, Michler J (2009) Brittle-to-ductile transition in uniaxial compression of silicon pillars at room temperature. Adv Funct Mater 19(15):2439–2444

[20] Zou Y, Kuczera P, Sologubenko A, Sumigawa T, Kitamura T, Steurer W, Spolenak R (2016) Superior room-temperature ductility of typically brittle quasicrystals at small sizes. Nat Commun 7:12261. https://doi.org/10.1038/ncomms12261

[21] Jang D, Greer JR (2010) Transition from a strong-yet-brittle to a stronger-and-ductile state by size reduction of metallic glasses. Nat Mater 9(3):215–219

[22] Goldman AI, Kong T, Kreyssig A, Jesche A, Ramazanoglu M, Dennis KW, Bud'ko SL, Canfield PC (2013) A family of binary magnetic icosahedral quasicrystals based on rare earths and cadmium. Nat Mate 12(8):714–718

[23] Canfield PC, Fisk Z (1992) Growth of single crystals from metallic fluxes. Philos Mag B 65(6):1117–1123

[24] Canfield PC, Kong T, Kaluarachchi US, Jo NH (2016) Use of frit-disc crucibles for routine and exploratory solution growth of single crystalline samples. Philos Mag 96(1):84–92

[25] Nishimoto K, Sato T, Tamura R (2013) Low-temperature superstructures of a series of Cd6 M (M = Ca, Y, Sr, Pr, Nd, Sm, Gd, Tb, Dy, Ho, Er, Tm, Yb and Lu) crystalline approximants. J Phys: Condens Matter 25(23):235403

[26] Flores K, Dauskardt R (2001) Mean stress effects on flow localization and failure in a bulk metallic glass. Acta Mater 49(13):2527–2537

[27] Ogata S, Shimizu F, Li J, Wakeda M, Shibutani Y (2006) Atomistic simulation of shear localization in Cu–Zr bulk metallic glass. Intermetallics 14(8):1033–1037

[28] Bharathula A, Lee S-W, Wright WJ, Flores KM (2010) Compression testing of metallic glass at small length scales: effects on deformation mode and stability. Acta Mater 58(17):5789–5796

[29] Howie PR, Korte S, Clegg WJ (2012) Fracture modes in micropillar compression of brittle crystals. J Mater Res 27(1):141–151

[30] Kraft O, Volkert C (2006) Size effects on deformation and fatigue of thin films and small structures. Cambridge University, Cambridge

[31] Schneider A, Kaufmann D, Clark B, Frick C, Gruber P, Mönig R, Kraft O, Arzt E (2009) Correlation between critical temperature and strength of small-scale bcc pillars. Phys Rev Lett 103(10):105501

[32] Uchic MD, Shade PA, Dimiduk DM (2009) Plasticity of micrometer-scale single crystals in compression. Ann Rev Mater Res 39:361–386

[33] Han SM, Bozorg-Grayeli T, Groves JR, Nix WD (2010) Size effects on strength and plasticity of vanadium nanopillars. Scr Mater 63(12):1153–1156

[34] Lee S-W, Nix WD (2012) Size dependence of the yield strength of fcc and bcc metallic micropillars with diameters of a few micrometers. Philos Mag 92(10):1238–1260

[35] Parthasarathy TA, Rao SI, Dimiduk DM, Uchic MD, Trinkle DR (2007) Contribution to size effect of yield strength from the stochastics of dislocation source lengths in finite samples. Scr Mater 56(4):313–316. https://doi.org/10.1016/j.scriptamat.2006.09.016

[36] Ng KS, Ngan AHW (2008) Breakdown of Schmid's law in micropillars. Scr Mater 59(7):796–799. https://doi.org/10.1016/j.scriptamat.2008.06.019

[37] Volkert CA, Donohue A, Spaepen F (2008) Effect of sample size on deformation in amorphous metals. J Appl Phys 103(8):083539. https://doi.org/10.1063/1.2884584

[38] Wang CC, Ding J, Cheng YQ, Wan JC, Tian L, Sun J, Shan ZW, Li J, Ma E (2012) Sample size matters for Al88Fe7Gd5

metallic glass: smaller is stronger. Acta Mater 60(13–14):5370–5379. https://doi.org/10.1016/j.actamat.2012.06.019

[39] Magagnosc D, Ehrbar R, Kumar G, He M, Schroers J, Gianola D (2013) Tunable tensile ductility in metallic glasses. Sci Rep 3:1096